Astron. Astrophys. 331, 372–382 (1998)

ASTRONOMY AND ASTROPHYSICS

The far infrared line spectrum of the protostar IRAS 16293-2422⋆

C. Ceccarelli[1,2], E. Caux[3], G.J. White[4], S. Molinari[2,5], I. Furniss[6], R. Liseau[7], B. Nisini[2], P. Saraceno[2], and L. Spinoglio[2], and M. Wolfire[8,9]

[1] Laboratoire d'Astrophysique, Observatoire de Grenoble - BP 53, F-38041 Grenoble Cedex 09, France
[2] CNR-Istituto di Fisica dello Spazio Interplanetario - CP 27, I-00044 Frascati, Italy
[3] CESR CNRS-UPS, BP 4346, F-31028 Toulouse Cedex 04, France
[4] Queen Mary and Westfield College, University of London, Mile End Road, London E1 4NS, UK
[5] LIDT, ISO Science Operations Centre, Villafranca, Spain
[6] University College, Gower St., London WC1E6BT, UK
[7] Stockholm Observatory, S-133 36 Saltsjöbaden, Sweden
[8] University of Maryland, College Park, MD 20742, USA
[9] Towson University, Department of Physics, Towson, MD 21252, USA

Received July 15 1997 / Accepted 10 October 1997

Abstract. We report mid-IR wavelength observations toward the low mass star forming region IRAS 16293-2422 between $45\mu m$ - $197\mu m$ with the Long Wavelength Spectrometer (LWS) on board ISO, and of the CI($609\mu m$) line observed with the JCMT. A map of the CII($157\mu m$) line shows that the region is relatively uncontaminated by Photo-Dissociation Region-like emission; there is only weak diffuse CII emission, which results from the illumination of the cloud by a faint UV field ($G_o \sim 6$). The observed CI($609\mu m$) line intensity and narrow profile is consistent with this interpretation.

On-source, the LWS detected the OI($63\mu m$) and several molecular lines. In this work we report and discuss in detail the lines which dominate the $43\mu m$ - $197\mu m$ spectrum, namely CO, H_2O and OH rotational lines and the OI($63\mu m$) fine-structure line. Combining the CO J_{up}=14 to 25 observations with previous J_{up}=6 measurements, we derive stringent limits on the density ($\sim 3 \cdot 10^4 cm^{-3}$), temperature ($\sim$1500 K), and column density ($\sim 1.5 \cdot 10^{20} cm^{-2}$) of the emitting gas. We show that this warm gas is associated with the outflow and that a low velocity, C-type shock can account for the characteristics of the CO spectrum.

If the observed H_2O and OH lines originate in the same region where the CO lines originate, the H_2O and OH abundance derived from the observed lines is [H_2O] / [H_2] $\sim 2 \cdot 10^{-5}$ and [OH] / [H_2] $\sim 5 \cdot 10^{-6}$ respectively. Given the relatively high temperature of the emitting gas, standard chemistry would predict all the gas-phase oxygen to be in water. The relatively low water abundance we observed may mean either that most of the oxygen is locked into grains or that the time scale required to convert the gas-phase oxygen into water is higher that the outflow time scale, or both. The relatively high abundance of OH with respect to H_2O gives support to the latter hypothesis.

Finally, we speculate that the OI($63\mu m$) line emission originates in the collapsing envelope that surrounds the central object. The successful comparison of the observed flux with model predictions of collapsing envelopes gives a mass accretion rate toward the central object $\geq 3 \cdot 10^{-5} M_\odot$ yr^{-1} and an accretion shock radius larger than three times the protostar radius.

Key words: ISM: jets and outflows – ISM: individual: IRAS 16293-2422 – stars: formation – infrared: ISM: lines

1. Introduction

It is widely accepted that low-mass stars form from the fragmentation and collapse of molecular clouds. In the process of contraction the gas warms up from an initial temperature of 10-20K, typical of dense clouds, to a few thousand of degrees, during the T-Tauri phase. During the first stages of protostellar formation the nearby gas is characterised by relatively low temperatures, and it therefore emits most of its energy at FIR wavelengths, between a few tens and a few hundred of microns.

The molecular cores, within which protostars form are illuminated by UV fields. This illumination may be external, either by the radiation of nearby young massive O B stars or by the local interstellar radiation field, and internal by the new born star. This UV illuminated gas is often termed a PhotoDissociation Region (PDR),and its far-IR spectrum is expected to be dominated by CII and other atomic fine structure line emission (Tielens & Hollenbach 1985). Depending on the UV field and

Send offprint requests to: C. Ceccarelli

⋆ Based on observations with ISO, an ESA project with instruments funded by ESA Member States (especially the PI countries: France, Germany, the Netherlands and the United Kingdom) with the partecipation of ISAS and NASA.

cloud density, the dynamics of the collapse can be strongly influenced in a sense by the characteristics of the radiation, which can accelerate the collapse or totally prevent it from happening (Lefloch & Lazareff 1995, Shematovich et al. 1997, Nelson & Langer 1997). Since most of a photon dominated cloud's mass is predicted to be contained in PDR-like halo (Nelson & Langer 1997), CII and atomic lines are expected to dominate the FIR line spectrum.

As the gas from the protostellar envelope collapses toward the central object, it is heated by compression, and by the accretion luminosity, whose combined effect may lead to temperatures of hundreeds degrees. Recently, Ceccarelli et al. (1996) modeled the chemical and thermal evolution of collapsing envelopes around low-mass protostars. In the innermost, warm regions of the envelope large amounts of water are expected to be formed, since it is both copiously formed in the gas phase, and is also released from grain mantles. In these regions, the infalling gas is cooled mainly by emission of the rotational lines of water. Further away from the protostar, the dust temperature drops below the critical temperature at which ice is evaporated from grains, and the gas-phase water abundance decreases. In these regions the OI($63\mu m$) fine structure line and CO rotational lines are the main coolants of the gas. All these lines can appear in emission *and* in absorption depending on the dust and gas temperature and the density profiles (see also Doty & Neufeld 1997).

Simultaneously with the collapse, matter also flows outwards from the central object. An overwhelming amount of data has been accumulated showing outflow phenomena, while very few observations have claimed to detect evidence of infall motion (Zhou 1992, Zhou 1995, Gregersen et al. 1997). Despite this large data collection on outflows, key information is still missing, in particular about the way an outflowing wind interacts with the surrounding medium. It is still a matter of debate whether a jet always drives the outflow and necessarly leads to the formation of bow shock structures (e.g. Raga & Cabrit 1993, Stahler 1994). By contrast, another class of models envisage wide angle collimated protostellar winds at the origin of the observed outflows (Shu et al. 1994, Li & Shu 1996). One of the outstanding general questions is how the high velocity outflowing velocity gas "travels" through the static circumstellar gas; either there is a continuous transition of the fluid properties, or a jump in the macroscopic gas quantities. In both cases, the gas is expected to emit copiously at FIR wavelengths, in both atomic fine structure lines and in molecular rotational lines (e.g. Hollenbach & McKee 1989; Kaufman & Neufeld 1996).

Unfortunately, the FIR wavelength range is mostly inaccessible to ground-based telescopes and barely accessible with airborne telescopes. For this reason just a handful of observations has been made toward low-mass Young Stellar Objects (YSOs), and in practice the observations have concentrated on the OI($63\mu m$) line, which was expected to be a bright line in many situations (Cohen et al. 1988, Ceccarelli et al. 1997). The launch of ISO has opened up the FIR window and now observations probing the gas around low-mass protostars are finally available (e.g. Nisini et al. 1996, Liseau et al. 1996, Saraceno et al. 1996a).

In this paper we report on observations of the FIR spectrum towards IRAS 16293-2422, one of the youngest objects so far known. We first review the information available about this source in Sect.2. The observations are described in Sect.3, and in Sect.4 we discuss the interpretation of the data and show how our results relate to the three phases mentioned above, i.e. the PDR, the infalling envelope and the outflow.

2. Source background

IRAS 16293-2422 is one of the best studied YSOs, and one in which infall has been claimed to occur simultaneously with outflow (Zhou 1995). It lies 160 pc away in a fairly isolated and cold molecular cloud core in the ρ Ophiuchus complex. The core contains two clumps of material separated by about $2'$(Wootten & Loren 1987, Mizuno et al 1990). The clump centered on the 27 $L_\odot$ source IRAS 16293-2422 is so deeply embedded that no emission has been detected at wavelengths shorter than $12\mu m$, against a strong millimeter emission, making it one of the youngest YSOs yet known; a so-called Class 0 object (André et al. 1993, Saraceno et al. 1996b). Radio and millimeter wavelength interferometric observations have shown that this IRAS source is actually a binary system, with two components, 1629a (in the southeast, with a mass $\sim$ 0.6 $M_\odot$) and 1629b (northwest, with a mass of $\sim$ 0.9 $M_\odot$), which lie $\sim$ 800 A.U. apart (Wootten 1989, Mundy et al. 1992, Walker et al 1993), and are embedded in an extended 4.5 $M_\odot$ dusty envelope ($40''$to $35''$) at 20K.

A molecular outflow toward IRAS 16293-2422 was independently discovered by Walker et al (1985), Fukui et al (1986), and Wootten & Loren (1987). Observations of the CO(J=2$\rightarrow$1) transition with higher spatial resolution have shown that this outflow has a quadrupolar shape (Walker et al 1988; Mizuno et al 1990), which has been interpreted as tracing two separated, almost perpendicular outflows emanating from 1629a and 1629b, respectively (Walker et al 1993). Ceccarelli et al. (1997) mapped the outflow in the OI($63\mu m$) line, deriving a mass loss rate of $2 \cdot 10^{-6} M_\odot yr^{-1}$. This is about 4 times less than that inferred from the CO measurements, implying a dynamical lifetime for the outflow a factor 4 times higher than has been previously assumed, i.e. $2 \cdot 10^4$yr.

3. Observations and results

3.1. ISO-LWS observations

Low resolution grating spectra covering the range from $43\mu m$ to $197\mu m$ were obtained during Revolution 85 (10th February 1996) with the ISO LWS. The observations consisted of a 4x3 grid of spectra covering a 400"x300" field of view, centered at $\alpha_{1950} = 16^h29^m24^s.6$, $\delta_{1950} = -24^\circ22'03''$ plus a deep integration centered on 1629a at the position $\alpha_{1950} = 16^h29^m20^s.9$, $\delta = -24^\circ22'13''$ (hereafter referred to as "on-source"). At each position 4 grating scans were taken with 0.25sec integration

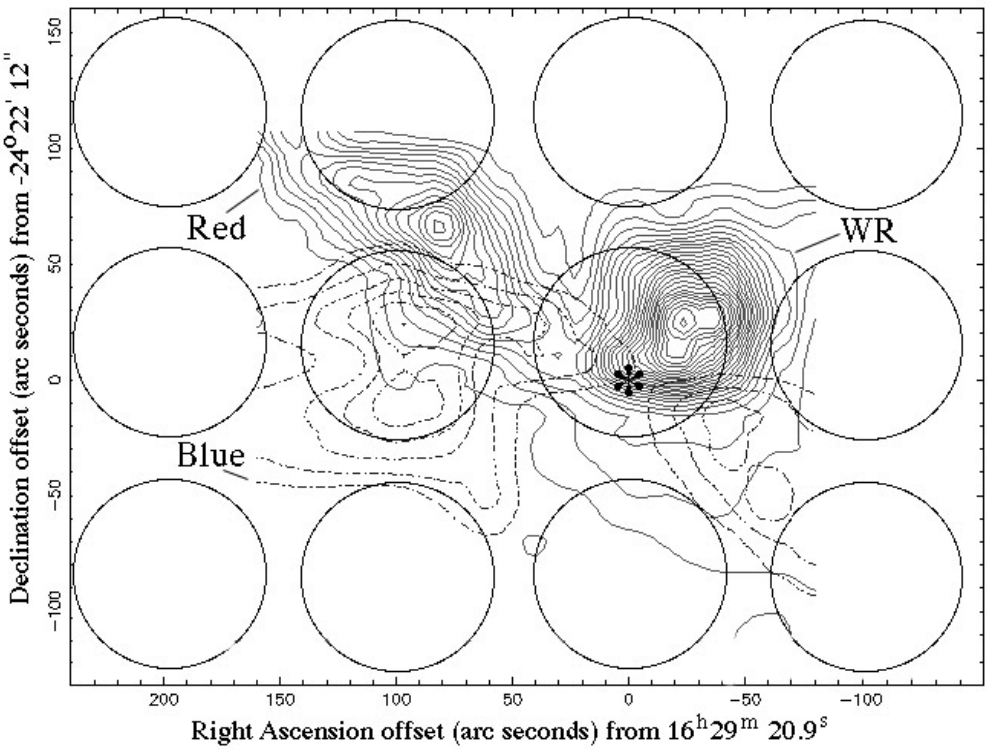

Fig. 1. Map of the ISO-LWS observations superimposed on the outflow mapped in the CO J=2→1 millimetre wave line (Ceccarelli et al. 1997b). The solid lines are the red-shifted emission while the dashed lines show the blue-shifted emission. The circles represents the beams of the LWS at the observed positions. The star shows the position of 1629a.

ramps per commanded grating position, sampled at 1/4 of a resolution element intervals. The total on target time for the map was 2509 seconds. The locations of the beams, and the half power beamwidths over the mapped region are shown in Fig.1, superimposed on the CO J=2-1 map of the outflow (Ceccarelli et al. in preparation).

We also obtained 16 grating scans at the on-source position, taken with 0.50 second integration ramps, over-sampled by a factor 4 , totaling a further 2509sec integration time. The spectra were flux calibrated using Uranus (Swinyard et al. 1996) and the absolute accuracy is estimated to be better than 30%. Finally, the LWS beamsize remains roughly constant at all wavelengths, $\sim$ 80" (Swinyard et al. 1996).

Emission from the CII($157\mu m$) line was detected at all positions in the map (Table1), with an average on-beam flux equal to $3.7 \cdot 10^{-12}$erg s^{-1} cm^{-2}. By contrast, the OI($63\mu m$) line was only detected on-source ($6.5 \cdot 10^{-12}$erg s^{-1} cm^{-2}), with 3σ upper limit $\sim 3 \cdot 10^{-12}$erg s^{-1} cm^{-2} elsewhere across the mapped region.

The map is undersampled because the beamsizes predicted before launch resulted larger than the observed ones. This does not have any impact on the discussion about the CII($157\mu m$) line emission, which results rather uniform. On the contrary, previous observations of the OI($63\mu m$) line show the presence of a strong emission peak 40″ west (Ceccarelli et al. 1997) of 1629A: we therefore re-did the map along the outflow. The discussion about the distribution of the line emission associated with the outflow will be reported in a forthcoming paper.

Besides the OI($63\mu m$) and CII($157\mu m$) lines, the more sensitive on-source observations detected several other molecular lines. The observed continuum plus line emission spectrum is shown in Fig.2. The line intensities are only a small fraction of the dust continuum intensity and are barely visible in this plot. To make them more visible we removed the continuum by subtracting second order polynomials between $90\mu m$ and $125\mu m$ and $125\mu m$ and $195\mu m$ respectively (note: this method used to remove the continuum does not have particular physical significance other than making the lines "visible": more detailed discussion of the continuum emission will be deferred to a later paper).

The resulting "continuum" subtracted line spectrum in the $90\mu m$ to $195\mu m$ range is shown in Fig. 3. Several lines become

Table 1. Diffuse CII($157\mu m$) Line Emission. The offsets are from the center of the map, $\alpha_{1950} = 16^h29^m24^s.6$, $\delta = -24°22'03''$.

Position		CII($157\mu m$) Flux
α	δ	(10^{-12}erg s^{-1}cm^{-2})
-150	-100	4.7 ± 0.7
-50	-100	3.9 ± 0.7
+50	-100	3.4 ± 0.7
+150	-100	3.3 ± 0.7
-150	0	4.1 ± 0.7
-50	0	3.0 ± 0.7
+50	0	3.4 ± 0.7
+150	0	3.3 ± 0.7
-150	+100	4.4 ± 0.7
-50	+100	3.5 ± 0.7
+50	+100	3.6 ± 0.7
+150	+100	3.8 ± 0.7

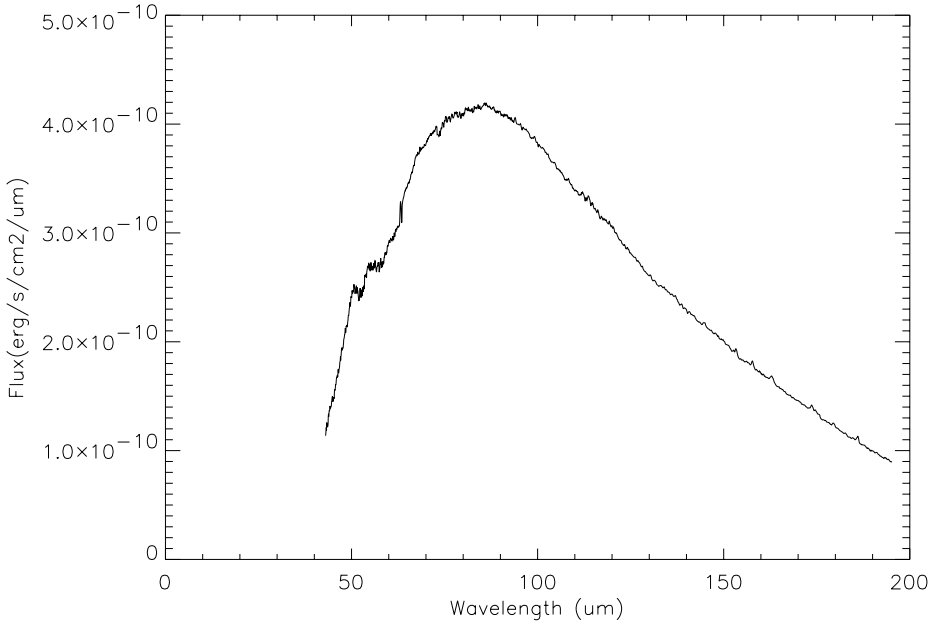

Fig. 2. On-source spectrum, showing both lines and the continuum flux.

clearly visible and the brightest of which are the CO, H_2O and OH lines indicated in the plot. At shorter wavelengths the line spectrum is dominated by the OI($63\mu m$) line which is shown in an expanded form in Fig. 4.

The CO, H_2O and OH line fluxes are reported in Table 2. These values were computed by defining a baseline around each line: this was relatively easy at $\lambda \geq 140\mu m$, but at shorter wavelengths the baseline removal was the main source of uncertainty. The statistical errors given in Table 2 are those due to the residuals from a gaussian fit to the fluxes, and the total error also takes into account uncertainty in the baseline determination.

Discussion of the several other molecular lines present in the spectrum will be included in a later paper. Here we note that the HD line visible in the spectrum at $112\mu m$ is due to the presence of this line in absorption in the spectrum of Uranus (Swinyard, private comunication): this was not yet corrected in the calibration procedure at the time of this analysis.

3.2. CI observations

In addition to the above data, observations of the CI($_3P^1 - _3P^0$) line at 609 μm were obtained toward the on-source position with the James Clerk Maxwell Telescope (JCMT). The telescope parameters are the following: HPBW=10", η_{mb}=0.43 and η_{fss}=0.64. The pointing was accurate to $\sim 1''$rms. The CI line, shown in Fig. 5, appears as a narrow line with a main beam brightness temperature, central velocity, half power linewidth of 6.6 K, 4.05 Km sec^{-1} and 1.1 Km sec^{-1} respectively. This is narrower than any other line so far seen towards IRAS 16293-2422, including the rare isotopomer $C^{17}O$ (Blake et al. 1994, van Dishoeck et al. 1995). It is unlikely that this is due to some characteristic of the receivers, since two other lines - H_2CO (491.968 GHz) and CH_3OH (492.279 GHz) were present at the edges of the CI spectrum, and these had line widths broader than that of CI, and typical of other lines detected in Blake et al.'s study.

Table 2. On-source observed line fluxes. The first column reports the observed line center, second column the observed fluxes with their statistical errors, third column the total error flux (see text) and fourth column the transition.

λ_{obs} (μm)	Flux 10^{-12}erg s^{-1} cm^{-2}	Error	Transition
63.20	6.5 ± 0.3	0.9	OI:$^3P_2 \rightarrow ^3P_1$
99.18	1.6 ± 0.3	0.6	OH:$^2\Pi_{1/2}5/2- \rightarrow ^2\Pi_{1/2}3/2+$
			o-H_2O:$5_{05} \rightarrow 4_{14}$
104.56	1.0 ± 0.3	0.6	CO:25→24
108.32	1.9 ± 0.5	0.9	o-H_2O:$2_{21} \rightarrow 1_{10}$
			CO:24→23
113.70	5.3 ± 1.0	2.5	CO:23→22
			o-H_2O:$4_{14} \rightarrow 3_{03}$
119.32	1.5 ± 0.2	0.5	OH:$^2\Pi_{3/2}5/2- \rightarrow ^2\Pi_{3/2}3/2+$
124.15	0.7 ± 0.2	0.5	CO:21→20
130.32	1.0 ± 0.3	0.6	CO:20→19
137.05	2.0 ± 0.3	0.9	CO:19→18
144.83	2.3 ± 0.3	0.7	CO:18→17
153.30	3.2 ± 0.3	0.7	CO:17→16
157.74	2.8 ± 0.3	0.6	CII:$^2P_{1/2} \rightarrow ^2P_{3/2}$
162.93	3.5 ± 0.3	0.6	CO:16→15
163.35	1.5 ± 0.3	0.8	OH:$^2\Pi_{1/2}3/2- \rightarrow ^2\Pi_{1/2}1/2+$
173.75	3.2 ± 0.3	0.6	CO:15→14
174.60	1.3 ± 0.3	0.6	o-H_2O:$3_{03} \rightarrow 2_{12}$
179.55	2.1 ± 0.2	0.6	o-H_2O:$2_{12} \rightarrow 1_{10}$
180.67	0.4 ± 0.2	0.3	o-H_2O:$2_{21} \rightarrow 2_{12}$
186.00	2.9 ± 0.2	0.6	CO:14→13

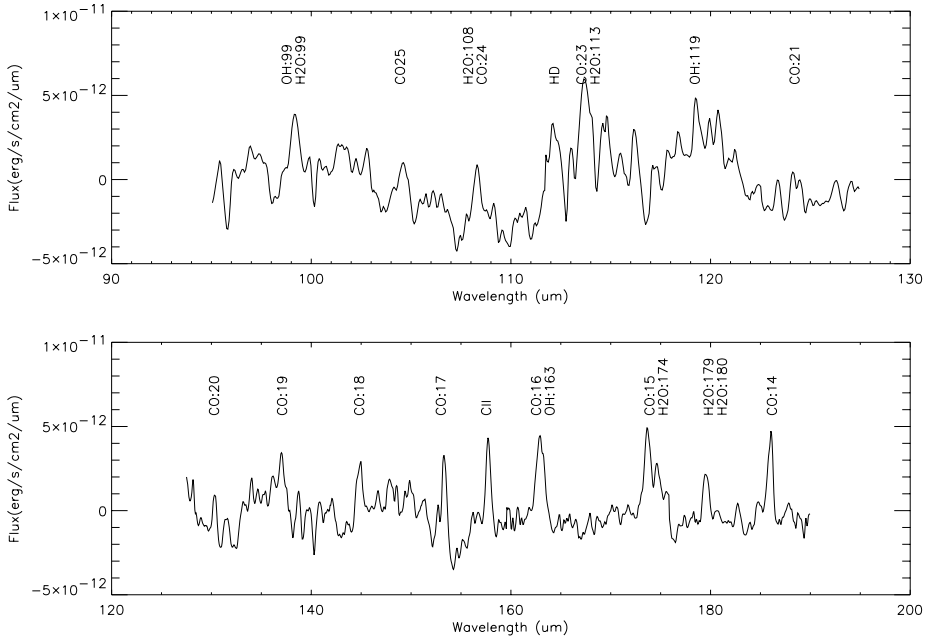

Fig. 3. On-source "continuum" subtracted line spectrum.

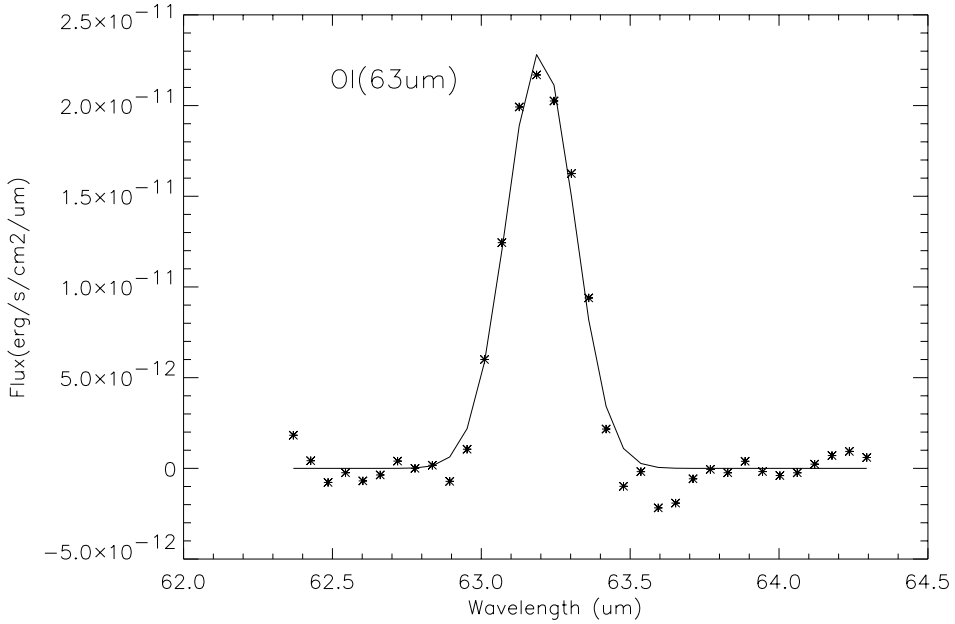

Fig. 4. On-source OI(63 μm) line: solid line shows the gaussian fit.

4. Discussion

4.1. The CII(157μm) and CI(609μm) line emission

CII(157μm) line emission was detected at a similar level at all positions in the mapped area, with a flux density $2.5{\cdot}10^{-5}$erg sec^{-1} cm^{-2} sr^{-1}, consistent with the upper limit reported by Yui et al (1993). Because of this lack of spatial structure, the origin of the CII(157μm) line emission is straightforward: it comes from UV illuminated gas belonging to the cloud, i.e. the so called PhotoDissociation Region (Tielens & Hollenbach 1985), and is not directly associated with IRAS 16293-2422 itself. Assuming the cloud density is $2{\cdot}10^3$cm^{-3} (Walker et al. 1990),comparison with the model results of Hollenbach et al. (1991, here after HTT91) suggests that the observed CII(157μm) lines are a consequence of a weak incident UV field with $G_o \sim 6$ (i.e. 6 times the interstellar UV field). Under these circumstances, which assume a filling factor of unity, $\sim 2.5\%$ of the incident energy is re-radiated as CII(157μm) line emission. According to the model, the OI(63μm) flux associated with this PDR region would be less than 2% of the CII(157μm) flux and hence undetectable by these observations. Therefore, we conclude that the OI(63μm) line detected at the on-source position does not originate in the PDR gas.

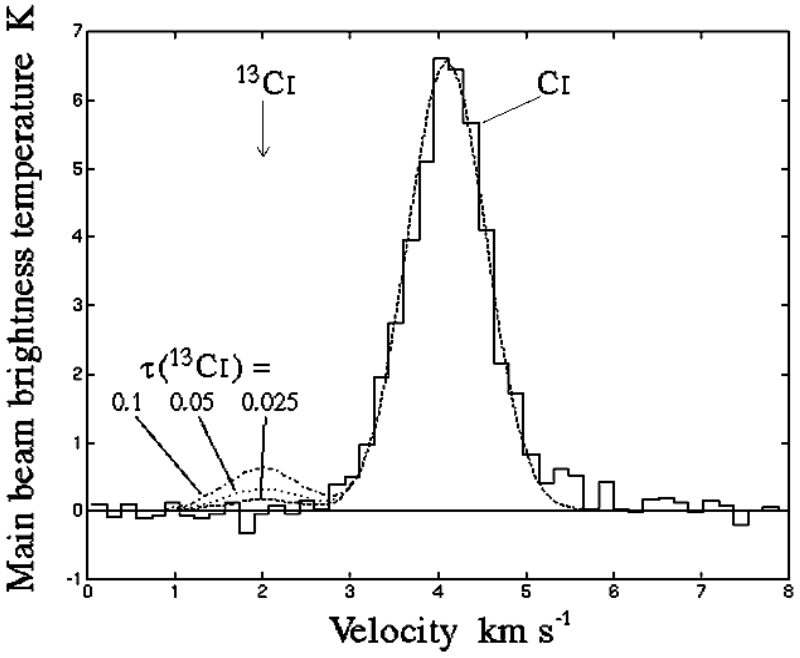

Fig. 5. The CI spectrum was obtained by coadding data from two JCMT receivers, RxC1 and RxC2, corrected to a common calibration scale. A gaussian model is superimposed onto the data, with a second line added at -2.2 km s-1, where the ^{13}CI line is expected. For this, the CI opacity is assumed to be much greater than 1, and the gas temperature is set (to match the data for unity filling factor) to 16 K, and with the ^{13}CI opacity set to values of 0.025, 0.05 and 0.1.

A comparison of the theoretical cooling rate of CII (HTT 1991) with the observed flux density F, allows the mass of the gas in the CII halo, M_{halo}, to be estimated . Assuming that the CII(157μm) line is optically thin and that [CII]/[H] is $3 \cdot 10^{-4}$ (i.e. all carbon is in this form), the mass of gas in the halo of the cloud is given by the relationship

$$M_{halo} = 1.6 \cdot \left(\frac{F[CII(157\mu m)]}{2.5 \cdot 10^{-5} erg\ s^{-1} cm^{-2}}\right) \left(\frac{\Omega}{300'' x 400''}\right) \left(\frac{3 \cdot 10^3 cm^{-3}}{n_{halo}}\right) \left(1 + \frac{1}{2} e^{92/T} (1 + \frac{n_{cr}}{n_{halo}})\right) M_\odot \quad (1)$$

Here, n_{halo} is the density in the CII halo, T is the gas temperature and n_{cr} is the critical density of the transition $\sim 2.8 \cdot 10^3 cm^{-3}$. Assuming an average gas temperature T of 20K (from the analytical expression for the gas temperature profile given by HTT91, Eq. 17: see also the gas temperature profile computed by Wolfire et al. 1990), then the halo mass within the 300"x400" area which has been observed is $\sim$ 2 $M_\odot$. However the assumed density n_{halo} is based on $C^{18}O$ observations and therefore refers to the molecular core. The density in the halo is rather difficult to estimate from the CII observations alone, since this line is relatively insensitive to the density in this range of G_0 values. Moreover, the CII abundance has to be regarded as an upper limit, as some of the carbon may be locked into grains. Consequently we consider 2 $M_\odot$ as a *lower limit* to the mass in the CII halo.

The PDR interpretation is also able to explain the narrow line profile observed in the CI(609μm) line, shown in Fig. 5. The beam-averaged, CI column density, N(CI) can be estimated using the relationship given by Keene (1990). Assuming the line is optically thin and has an excitation temperature of 20 K, we find N(CI) = 1.1 10^{17} cm^{-2}, in excellent agreement with the predictions of the HTT91 model described above. This estimate is relatively insensitiveto the choice of the excitation temperature over a reasonable range.

The CI line is sufficently narrow that the ^{13}CI isotopomer, which lies 3.6 MHz higher in frequency (or at a relative velocity of -2.2 Km sec^{-1}) from the CI line, could just be resolved if it were present. Taking the upper limit to the intensity of the J=1-0 F$\rightarrow$ F' = 3/2 - 1/2 ^{13}CI line from Fig. 5, the ^{13}CI opacity can be estimated to first order using the relationship:

$$\frac{T_{mb}(^{13}CI)}{T_{mb}(^{12}CI)} = \frac{1 - e^{-\tau(^{13}CI)}}{1 - e^{-\tau(^{12}CI)}} \quad (2)$$

From the data, we estimate $\tau(^{13}CI) \leq 0.025$. This can then be used with Keene (1990) expression to set upper limits to the ^{13}CI column density, N(^{13}CI) $\leq$ 1.5 $10^{15} cm^{-2}$, and a lower limit to the abundance ratio [^{12}CI]/[^{13}CI] $\geq$ 73. This is consistent with theoretical chemistry models that predict [^{12}CI]/[^{13}CI] $\geq$ 160, for densities higher than $3 \cdot 10^3 cm^{-3}$ and [C]/[O] ratios in the range 0.42 and 1.28 (Langer et al. 1984). However, Keene (private communication) has reported [^{12}CI]/[^{13}CI]$\sim$53 towards the Orion region. Our upper limit to the ^{13}CI temperature in IRAS 16293-2422 would appear to be somewhat below her detection in Orion.

4.2. The molecular line emission

Beside the CII(157μm) and OI(63μm) lines, the on-source LWS spectrum shows CO rotational transitions from J_{up} of 14 through to 25, and rotational transitions of ortho-H_2O and OH.

An LVG model, applied to a slab geometry, was used to interpret the observed CO line intensities. This model considers the first 50 rotational levels, with the collisional excitation rates taken from McKee et al (1982) and an adopted value for

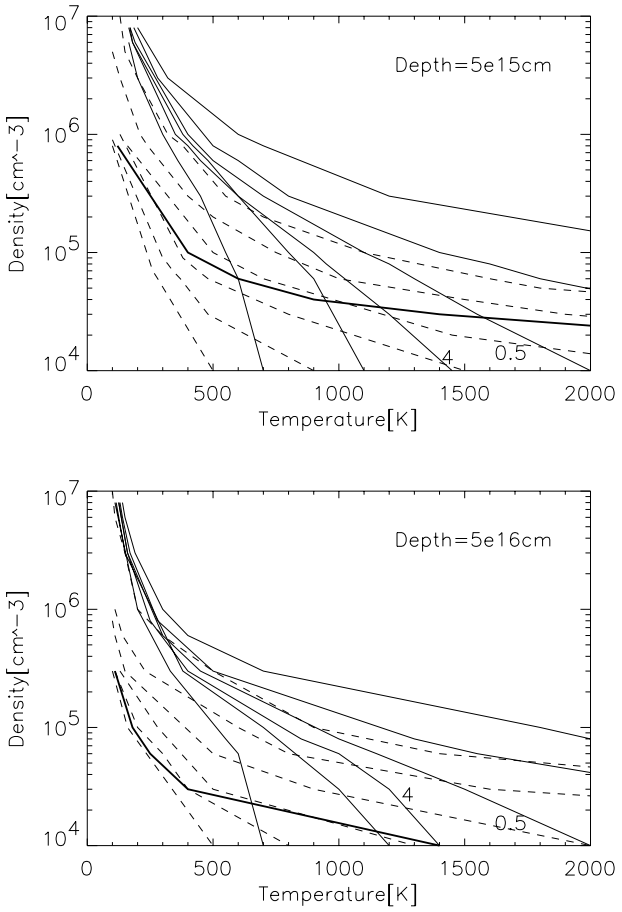

Fig. 6. Theoretical CO line ratios for two different slab depths: $5 \cdot 10^{15}$ cm (top panel) and $5 \cdot 10^{16}$ cm (bottom panel): these two values were chosen because they give lines optically thin ($5 \cdot 10^{15}$ cm case) or thick ($5 \cdot 10^{16}$ cm case), and therefore represent two possible extreme situations. Solid lines represent the 14→13 to 21→20 line ratio: from the top to the bottom the values are 1.0, 2.0, 3.0, 4.0, 5.0 and 10. The observed value equal to 4 is indicated. Dashed lines represent the 6→5 to 14→13 line ratio: from the top to the bottom the values are 0.1, 0.2, 0.5, 1.0, 2.0 and 5.0.The observed value equal to 0.5 is indicated. The bold line represents the density and temperature values for which the predicted flux will be equal to the observed flux, i.e. $4 \cdot 10^{-12}$erg $s^{-1}cm^{-2}$, in the J=14→13 transition assuming a source size of 14"x80" (see the text).

[CO] / [H_2] = 10^{-4} (van Dishoeck et al 1995). Additionaly, the linewidth is assumed to be 10 km s^{-1}, as suggested by the CO J=6→5 of Ceccarelli et al (in preparation). The model has four other free parameters: the density and the temperature of the gas, the angular extent of the emitting region and the depth of the slab (multiplied by the linewidth). The last two parameters, the angular extent and slab depth, are independent only if the lines are optically thick, otherwise the emission is proportional to their product.

The theoretical CO J=14→13 to J=21→20 line ratio as a function of the density and temperature of the gas are shown in Fig. 6. The top panel shows the computation for a slab depth of $5 \cdot 10^{15}$ cm and the bottom panel shows the $5 \cdot 10^{16}$ cm thick case. The former value of the slab depth predicts optically thin lines and therefore any value of linewidth greater than 10 km s^{-1} or slab depth less than $5 \cdot 10^{15}$ cm would give the line ratios of top panel. The $5 \cdot 10^{16}$ cm case represents an extreme large value at which the lines start to become optically thick.

The observed 14→13-to-21→20 ratio to compare with these figures is 4±2 (marked in Fig.6). It is evident from Fig.6 (when considering *only* the solid curve marked 4) that the CO lines observed by the LWS cannot uniquely constrain the parameters of this model, and only put a lower limit to the gas temperature $\geq$ 150K. The emission could, in principle, be explained as either originating in a dense ($\sim 10^7 cm^{-3}$), compact ($\sim 8 \cdot 10^{15}$ cm) and warm ($\sim$ 150 K) gas, *or* to arise in less dense ($\sim 10^4 cm^{-3}$), more diffuse ($\sim 10^{17}$cm) and hotter ($\sim$ 2000 K) gas. However, the denser and colder hypothesis seems to be unlikely, since in this case the gas and dust will be thermally coupled and a 30 $L_\odot$ source would only heat the dust (and consequently, the gas) up to $\leq$ 50 K at $r \sim 10^{16}$cm. It seems unlikely that CO line emission would escape self-absorption by colder gas, lying further outer the surrounding envelope. In fact, detailed model computations of CO emission lines from collapsing envelopes predict a very high opacity for the high J CO lines, and, consequently, a much lower flux (Ceccarelli et al. 1996).

Additional support for the hot diffuse hypothesis is provided by observations made in the CO J=6→5 transition toward IRAS 16293-2422 (Ceccarelli et al, in preparation). The observed CO J=6→5 emission is extended about 14"x80" and both the broadened line profiles and the spatial distribution clearly suggest that the CO J=6→5 emission originates in the outflowing gas. Assuming that the high J CO emission observed comes from the same region, we can set stringent limits to constrain inputs to the LVG model. The dashed lines of Fig.6 show the theoretical J=6→5 to J=14→13 flux ratio: the observed value is 0.5±0.3. Also, in Fig.6 we show the densities and temperatures that would give a J=14→13 flux equal to the observed one, assuming the emitting gas extent to be equal to 14"x80" (bold line). Now the intersection of the 4 solid line (14→13 to 21→20 flux ratio), the 0.5 dashed line (6→5 to 14→13 flux ratio) and the bold line impose stringent constraints to the remaining three parameters of the model, i.e. the density and temperature of the gas and the depth of the slab. The J=6→5 to J=25→24 CO lines are fitted by gas with a density between $3 \cdot 10^4$ cm^{-3} and $4 \cdot 10^4$ cm^{-3}, a temperature between 1000 K and 1700 K, and a slab depth $\sim 5 \cdot 10^{15}$ cm. The CO column density of this warm gas is then $\sim 1.5 \cdot 10^{16}$ cm^{-2} and the mass is $\sim 2 \cdot 10^{-3}$ $M_\odot$. The total CO line observed luminosity in this case amounts to 0.04 $L_\odot$, i.e. 10^{-3} of the bolometric luminosity of the source. The fitted spectrum is shown in Fig. 7.

We also used an LVG code to interpret the H_2O and OH line intensities, by solving the transfer equations for 48 and 44 levels respectively. The spontaneous emission coefficients are taken from the HITRAN database (Rothman et al. 1987), the H_2O collisional coefficients from Green et al. (1993) and the OH rates from Offer et al. (1994). Assuming that the water lines originate in the same hot gas where the CO lines originate,

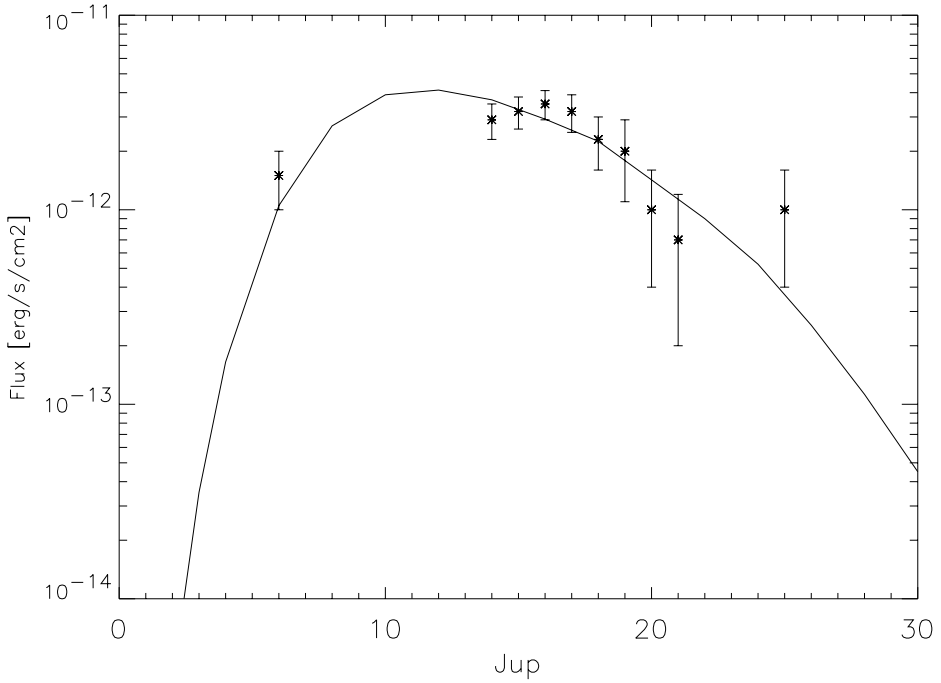

Fig. 7. The best fit of the CO line spectrum. The ISO-LWS points with $J_{up} \geq 14$ are presented in this work, while the J=6→5 line is from Ceccarelli et al. (1997b). The solid line shows the emission of a slab of gas at a temperature of 1500 K and with a volume density of $3 \cdot 10^4$ cm^{-3}. The depth of the slab for this calculation is $5 \cdot 10^{15}$ cm.

the $[H_2O]/[H_2] = 2 \cdot 10^{-5}$. We emphasise that it is *not* possible to exclude a different origin for these lines, given the detection of only a few water lines. Neverthless, the upper limit on the $75\mu m$ line (the $3_{2,1} \rightarrow 2_{1,2}$ transition) flux ($\leq 3 \cdot 10^{-12}$ erg s^{-1}cm^{-2}) firmly rules out the colder and denser hypothesis, i.e. that the H_2O emission originates in gas at density $\sim 10^7$cm^{-3} and temperature $\sim$ 150 K: in this case the $75\mu m$ line would be about 10 times larger than the $179\mu m$ line, an hypothesis not supported by the observational data.

Finally, assuming that the observed OH line emission also originates from the hot gas responsible for the CO emission, the $[OH]/[H_2] \sim 5 \cdot 10^{-6}$, i.e. the OH abundance is only 4 times lower than the H_2O abundance.

4.3. The C-shock associated with the outflow

It has already been suggested that the CO J=6→5 line emission originates in the outflow, both from considerations of the line shape and the spatial distribution. Consequently, the higher J transitions seen in LWS will also originate in the outflow. It is natural to think that the observed CO emission comes from material associated with the interaction of the stellar wind emanating from the central star with the ambient medium. There are at least three reasons that lead to the hypothesis that this interaction will be better described by a C-shock (Draine 1980) than a J-shock (Hollenbach & McKee 1989).

First, the OI($63\mu m$) luminosity observed on-source is a factor 10 lower than the observed molecular line emission. In J-shocks atomic lines are expected to be the major coolants throughout most of the postshock region, while molecular emission would only arise from a smaller region. As a consequence, OI($63\mu m$) is expected to be more luminous than CO emission. In C-shocks, the opposite is true: molecules are the main coolants and very little atomic line emission is expected, if at all.

A second argument in favor of C-shocks is the relatively high gas temperature ($\sim$ 1500 K). Although J-shocks produce relatively higher temperatures ($\sim 10^5$K), molecules, destroyed by the harsh environment behind the shock front, will reform in a region far enough downstream that the UV radiation is attenuated, where the gas temperature falls to $\sim$ 400 K (the so-called "H_2 plateau": Hollenbach & McKee 1989). By contrast, in C-shocks the gas will be heated to much lower temperatures ($\lesssim 3000K$), where not only are most molecules not destroyed, but some (like water) are copiously formed (e.g. Graff & Dalgarno 1987).

A third argument is the relatively low density ($\sim 3 \cdot 10^4$cm^{-3}). In J-shocks the emission originates when the gas is already compressed and the compression factor is expected to be $\sim$ 100. As a consequence, very low pre-shocks densities would be expected, which imply that no appreciable molecular emission would be detected (as there is no formation of the H_2 plateau: Hollenbach & McKee 1989). Again, in C-shocked gas the compression factor is lower and the emission originates predominantly in the region where the gas is being compressed.

However, these scenarios point to an inconsistency in explaining the observations in terms of C-shock models. Given the high temperature ($\sim$ 1500K) of the emitting gas, "standard" chemical models predict that all the oxygen (not in CO) will be locked into water molecules, as the endothermic reaction O + H_2 → OH + H followed by OH + H_2 → H_2O + H would efficiently incorporate the atomic oxygen into water molecules (Graff & Dalgarno 1987).

On the other hand, we only see $[H_2O]/[H_2] \sim 2 \cdot 10^{-5}$. This means that either a relevant fraction of the gas-phase oxygen is in

forms other than water, or that it is locked into the the icy mantles of grains, or both. The OI($63\mu m$) on-source line intensity would require an atomic oxygen abundance [OI]/[H_2] $\sim 2.5 \cdot 10^{-5}$ if it originates in the same region as the CO, H_2O and OH emission (the OI($63\mu m$) line results optically thin under these conditions). So even assuming that not all gas-phase oxygen is locked into water, a large fraction of oxygen must be in other molecules, such as O_2 (for which is difficult to obtain stringent upper limits on the abundance). In principle, if the pre-shock gas is not fully molecular but mainly atomic, as some protostellar wind models predict (see for example Glassgold et al. 1991), the timescale for conversion of all the oxygen into water may exceed the "outflow dynamical time" (see for example the time dependent computation of Graff & Dalgarno 1987). Indeed the observed high OH abundance with respect to the H_2O abundance provides support to this hypothesis.

However, there is also a simpler explanation for the relatively low observed water abundance. Although the gas is heated by the shock, the same does not necessarily apply to the dust grains, whose temperature may well be less than the ice evaporation limit of $\sim$ 100 K. Hence, a simple explanation for the relatively low water abundance is that the oxygen may be locked into grain mantles.

Anyway, this would not explain the high [OH]/[H_2O] observed ratio which clearly demostrates that the conversion of OH onto H_2O has not yet been completed, and that the chemical timescale exceeds the outflow dynamical scale. This also implies that the pre-shock gas is not fully molecular. Forthcoming observations which are planned with ISO to observe the H_2 rotational lines at longer wavelengths may bring some light on this issue.

In conclusion, the observed molecular emission agrees with the general characteristics predicted by C-shock models. However, a detailed comparison with any specific model that depends on a relatively large number of input parameters is beyond the scope of this paper. Such mild shocks may be result of the oblique impact of a wind with the edges of the cavity wall created by the wind itself, or they may represent the tails of a bow shock, or finally they may trace the entraintenement of the ambient material by the wind. Model computations by Lizano & Giovannardi (1995), although explicitly "tuned" for the L1551 outflow, predict that the mixing layers of the material entrained along the cavities of an outflow would attain temperatures of up to several thousand degrees.

4.4. The on-source OI($63\mu m$) line emission and the infall

Finally, we would like to explore the possibility that the OI($63\mu m$) line emission observed at the on-source position originates in the collapsing envelope sourrounding IRAS 16293-2422. Recently Ceccarelli et al. (1996) modeled the infalling protostellar envelopes, computing self-consistently the evolution of their chemical and thermal structure and the emitted line spectrum. This model used the inside-out collapse picture developed by Shu (1977). Their model predictions are sensitive to five key parameters: the source luminosity, accretion shock radius (where the gravitational energy is released in the shock), the mass accretion rate and the gas-phase water and CO abundances. The water abundance does not significatively affect the predicted OI($63\mu m$) line luminosity, as this line originates in a part of the envelope where the CO and OI are the main coolants of the gas. Since we have independent measurements of the CO abundance and the bolometric luminosity, the computed OI($63\mu m$) line luminosity only depends on the accretion shock radius and the mass accretion rate.

We show in Fig.8 the predictions of this model for a source of 30 $L_\odot$ as a function of the mass accretion rate for three different values of accretion shock radius.

The agreement with the observed value is striking: the model predictions are consistent with the observed OI($63\mu m$) emission for the mass accretion rates $\geq 2 \cdot 10^{-5}$ $M_\odot yr^{-1}$ and accretion shock radii larger than 3 times the protostar radius.

We are conscious that this interpretation is still speculative and that high spectral resolution observations of the OI($63\mu m$) line are needed to assess if the origin of this line is in gas associated with the collapsing envelope or from the outflow. However, the point at $3 \cdot 10^{-5}$ $M_\odot yr^{-1}$ and accretion shock radii equal to 0.4 AU corresponds to the model which also fits the observed CS line profiles (Zhou 1995). The same model predicts CO lines about a factor ten lower than the observed ones, while the H_2O predicted lines are a factor four lower than the observed ones, assuming a water abundance of [H_2O]/[H_2]=10^{-4}. This agrees with the hypothesis discussed in the previous section that CO emission originates in the shock created by the interaction of the protostellar wind with the surrounding medium.

Given the uncertainty on the water abundance, we cannot therefore exclude the infalling envelope as an origin of the observed water lines (but unfortunately we cannot conclude that they do, either). Should it be the case, the arguments of the previous section about the H_2O formation in C-shocks would anyway be valid (in fact the quoted H_2O abundance should be considered as an upper limit).

5. Conclusions

Observations are presented towards IRAS 16293-2422 with the ISO-LWS over the $43\mu m$-$197\mu m$ range, and the CI ($609\mu m$) line obtained with JCMT.

The LWS observations reveal the presence of weak, diffuse and uniform CII($157\mu m$) emission over a 400"x300" area around the IRAS source. The on-source CI line shows a very narrow profile, probing the quiescent material around the source. Both lines are well explained as due to PDR emission of the cloud illuminated by a low UV field, $G_0 \sim 6$.

On-source we observed a rich $43\mu m$-$197\mu m$ molecular spectrum, dominated by the OI($63\mu m$) line and the CO, H_2O and OH rotational lines.

We combine the high J CO emission together with the CO J=6$\rightarrow$5 observed by Ceccarelli et al. (in preparation) to place stringent limits on the density, temperature and column density of the emitting gas. The best fit to the observed CO spectrum from J_{up}=6 to J_{up}=25 is obtained with a density value of $3 \cdot 10^4$

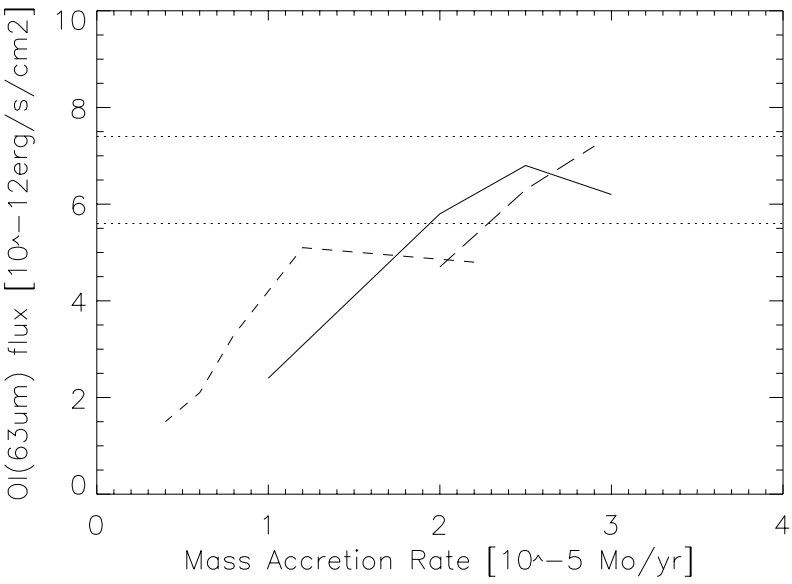

Fig. 8. OI($63\mu m$) line flux versus mass accretion rate. The short dashed line referes to an accretion shock radius equal to the protostar radius (following to Stahler 1988), the solid line assumes that the accretion shock radius is 3 times the protostar radius, and finally the long dashed line assumes that the accretion shock radius is ~ 0.4 AU. The dotted lines show the range of the observational limits, taking into account a 30% uncertainty.

cm^{-3}, a temperature $\sim$ 1500 K and a CO column density of $1.5{\cdot}10^{16}$ cm^{-2}. A low velocity, C-type shock is the cause for the heating of the gas.

The observed water line fluxes are consistent with a water abundance [H_2O]/[H_2]=$2{\cdot}10^{-5}$. This low water abundance may indicate that a large fraction of oxygen is locked onto grains. The OH abundance derived by the observed fluxes is only four times lower than the H_2O abundance: this suggests that the timescale to convert the gas-phase atomic oxygen and OH into water is larger than the outflow dynamical scale, implying that the protostellar wind is not fully molecular.

Finally we speculate on the origin of the OI($63\mu m$) line emission as due to the thermal emission of the collapsing envelope.

Acknowledgements. CC wishes to wholeheartedly thank D. Hollenbach for his stimulating comments to a draft version of this paper. It is also a pleasure to thank E. van Dishoeck for providing us with the OH collisional rates in an electronic format and R. Padman for the help in the CI observations. We finally thank our referee, B. McCutcheon, for carefully reading and commenting the paper.

References

André P., Ward-Thompson D., Barsony, M., 1993, ApJ 406, 122
Blake.G.A, van Dishoeck E., Jansen D.J., Groesbeck T.D., Mundy, L.G. 1994, ApJ 428, 680
Ceccarelli C., Hollenbach D.J., Tielens A.G.G.M., 1996, ApJ 471, 400
Ceccarelli C., Haas M.R., Hollenbach D.J., Rudolph A.L., 1997, ApJ 476, 771
Cohen M., Hollenbach D,J,, Haas M.R., Erickson E.F., 1988, ApJ 329, 863
van Dishoeck E.F., Blake G.A., Jansen D.J., Groesbeck T.D., 1995, ApJ 447, 760
Doty S.D., Neufeld D.A., 1997, ApJ, in press
Draine, B.T., 1980, ApJ 241, 1021
Fukui Y., Sugitani K., Takaba H., et al. 1986, ApJ 311,L85
Glassgold A.E., Mannon G.A., Huggins P.J., 1991, ApJ 373, 254
Graff M.M., Dalgarno A., 1987, ApJ 317, 432
Green S., Malauendes S., McLean A.D., 1993, ApJS 85, 181
Gregersen E.M., Evans N.J.II, Zhou S., Choi M., 1997, ApJ 484, 256
Hollenbach D.J. ,Tielens A.G.G.M. Takahashi, T., 1991 (HTT91), ApJ 377,, 192
Hollenbach D.J., McKee C.F., 1989, ApJ 342, 306
Kaufman M.J., Neufeld D.A., 1996, ApJ 456,611
Keene J., 1990, in: Proceedings of SETI conference "Carbon in the Galaxy: Studies from Earth and Space", p 181-196 (SEE N90-27562 21-88)
Langer W.D., Graedel T.E., Frerking M.A., Armentrout, P.B., 1984, ApJ 277, 581
Lefloch B., Lazareff B., 1995, A&A 301, 522
Li Z.Y., Shu F.H., 1996, ApJ 468, 261
Liseau R., Ceccarelli C., Larsson B., 1996, A&A, 315, L181
Lizano S., Giovannardi C., 1995, ApJ 447, 742
McKee C.F., Storey J.W.V., Watson D.M., Green S., 1982, ApJ 259, 647
Mizuno A., Fukui Y., Iwata T., Nozawa S., Takano T., 1990, ApJ 356, 184
Mundy L.G., Wootten A., Wilking B.A., Blake G.A. Sargent A.I., 1992, ApJ 385, 306
Nelson R.P., Langer W.D., 1997, ApJ 482, 796
Nisini B., Lorenzetti D., Cohen M. et al, 1996, A&A, 315, L32
Offer A.R., van Hemert M.C., van Dishoeck E.F., 1994, J.Chem.Phys. 100, 362
Raga A., Cabrit S., 1993, A&A 278, 267
Rothman L.S. et al, 1987, Appl. Opt. 26, 4058
Saraceno P., Ceccarelli C., Clegg P.E. et al, 1996a, A&A, 315, L293
Saraceno P., Andre' P., Ceccarelli C., Griffin M., Molinari S., 1996b, A&A 309, 827
Shematovich V., Shustov B., Wiebe D., 1997, A&A preprint
Shu F.H., 1977, ApJ 214, 488
Shu F.H., Najita J., Ruden S., Lizano S., 1994, ApJ 429, 797
Stahler S.W., 1988, ApJ 332, 804
Stahler S.W., 1994, ApJ 422, 616
Swinyard B.M., Clegg P.E., Ade P.A.R. et al., 1996, A&A 315, L43
Tielens A.G.G.M., Hollenbach D.J., 1985, ApJ 291, 747

van Dishoeck E.F., Blake G.A., Jansen D.J., Groesbeck T.D., 1995, ApJ 447, 760
Walker C., Lada C.J., Young E.T., Margulis M., Wilking B.A., 1985, BAAS 17, 835
Walker C., Lada C.J., Young E.T., Margulis M., 1988, ApJ 332, 335
Walker C.K., Carlstrom J.E., Bieging J.H., Lada C.J., Young E.T., 1990, ApJ 364, 173
Walker C., Carlstrom J.E., Bieging J.H., 1993, ApJ 402, 655
Wolfire M.G., Tielens A.G.G.M., Hollenbach D.J., 1990, ApJ 358, 116
Wootten A., 1989, ApJ 337, 858
Wootten A., Loren R.B., 1987, ApJ 317, 220
Yui Y.Y., Nakagawa T., Doi Y., et al., 1993, ApJ 419, L37
Zhou S., 1992, ApJ 394, 204
Zhou S., 1995, ApJ 442, 685

This article was processed by the author using Springer-Verlag LaTeX A&A style file *L-AA* version 3.